Available online at www.sciencedirect.com

SCIENCE DIRECT

Biochimica et Biophysica Acta 1763 (2006) 226–237

BIOCHIMICA ET BIOPHYSICA ACTA

BBA

http://www.elsevier.com/locate/bba

Dynamic relocation of poly(ADP-ribose) glycohydrolase isoforms during radiation-induced DNA damage

Jean-François Haince [a], Marie-Eve Ouellet [a], Darin McDonald [b], Michael J. Hendzel [b], Guy G. Poirier [a,*]

[a] *Health and Environment Unit, Laval University Hospital Research Center, CHUQ, Faculty of Medicine, Laval University, Room RC-9700, 2705 Laurier blvd., Ste-Foy, Québec, Canada G1V 4G2*

[b] *Department of Oncology, Faculty of Medicine, University of Alberta and Cross Cancer Institute, Alberta, Canada*

Received 30 August 2005; received in revised form 23 November 2005; accepted 28 November 2005
Available online 27 December 2005

Abstract

Poly(ADP-ribosyl)ation is a very early cellular response to DNA damage. Poly(ADP-ribose) (PAR) accumulation is transient since PAR is rapidly hydrolyzed by poly(ADP-ribose) glycohydrolase (PARG). PARG may play a prominent role in DNA damage response and repair by removing PAR from modified proteins including PARP-1. Using living cells, we provide evidence that in response to DNA damage induced by γ-irradiation the cytoplasmic 103 kDa PARG isoform translocates into the nucleus. We further observed that the nuclear GFP-hPARG110 enzyme relocalizes to the cytoplasm in response to DNA damage. Using different GFP-PARG fusion proteins specific for the nuclear and cytoplasmic forms, we demonstrate their dynamic distribution between cytoplasm and nucleoplasm and a high mobility of major PARG isoforms by fluorescence recovery after photobleaching (FRAP). The dynamic relocation of all PARG isoforms presented in this report reveals a novel biological mechanism by which PARG could be involved in DNA damage response.

Keywords: Poly(ADP-ribose) glycohydrolase; Poly(ADP-ribose); FRAP; Nucleocytoplasmic shuttling; Subcellular localization; DNA damage

1. Introduction

Poly(ADP-ribosyl)ation is a post-translational protein modification involved in DNA repair [1], apoptosis [2,3], transcription [4,5] and chromosome stability [6]. The formation of this unique biopolymer is catalyzed mainly by the nuclear enzymes poly(ADP-ribose) polymerase 1 (PARP-1) [7] and 2 (PARP-2) [8,9] but some catalysis also occurs through less abundant PARPs family members (for a review see [10]). Upon binding to DNA breaks, PARP-1 and PARP-2 are selectively activated and within seconds synthesize large amounts of a highly negatively charged PAR lattice on a variety of nuclear proteins including themselves [7]. The removal of PAR from the modified proteins is catalyzed by an enzyme, the poly(ADP-ribose) glycohydrolase (PARG), which is encoded by a single gene [11]. PARG possesses an exo- and endoglycosidase activity that rapidly hydrolyzes PAR.

The PARG gene and structure/function relationships have been recently characterized in different species [12–19]. It has been demonstrated that the gene encoding human PARG is alternatively spliced to generate three different protein isoforms with molecular weights of, respectively, 110, 103 and 99 kDa [18]. Expression of those multiple PARG isoforms has been positively confirmed in different human and mouse cell lines [14,18,20,21]. While some authors have shown the presence of a full-length 110 kDa PARG gene product in mammalian cells [14,18], only a limited number of studies have presented significant biological data or biochemistry describing the full-length 110 kDa human PARG. Previous studies have shown that the overexpressed full length PARG110 localizes predominantly to the nucleus [18,22], while PARG103 and PARG99 isoforms are cytoplasmic [18,23]. Interestingly, the cytoplasmic PARG103 isoform accounts for nearly 90% of the entire cellular activity [23]. The PARG enzyme contains a C-terminal catalytic

* Corresponding author. Tel.: +1 418 654 2267; fax: +1 418 654 2159.
E-mail address: guy.poirier@crchul.ulaval.ca (G.G. Poirier).

0167-4889/$ - see front matter © 2005 Elsevier B.V. All rights reserved.
doi:10.1016/j.bbamcr.2005.11.015

domain and a N-terminal putative regulatory domain (Fig. 1A) which would be involved in protein–protein interactions [24]. Furthermore, our group has completed the proteomic characterization of PARG-interacting proteins and found that PARG103 and 110 are component of a multi-protein complex involved in mRNA processing [25]. Moreover, a recent report demonstrated that the amino acid residues ^{10}CTKRPRW^{16} encoded by exon 1 of human PARG comprise a functional nuclear localization signal (NLS) that targets PARG to the nucleus [18], while other alternative NLS motifs have also been reported in the C-terminal catalytic domain (Fig. 1A) [16]. Importantly, all PARG isoforms, like PARP-1, has been found to be efficiently cleaved by caspase-3 in human cells undergoing apoptosis [21]. This cleavage of PARG releases two enzymatically active C-terminal fragments of 85 and 74 kDa and these PARG85 and PARG74 apoptotic fragments are also localized in the cytoplasm [23].

Apart from these observations, little is known about the biological significance of the cellular localization and the presence of different PARG isoforms other than they are able to catalyze PAR turnover in different cell compartments. The basal levels of polymer within unstimulated cells are usually very low [26–29] and the nuclear concentration in mammalian cells is usually within the range of one to two times the K_m value of PARG [30]. Therefore, the nuclear PAR concentration is sufficient to maintain a constant PARG activity, even in

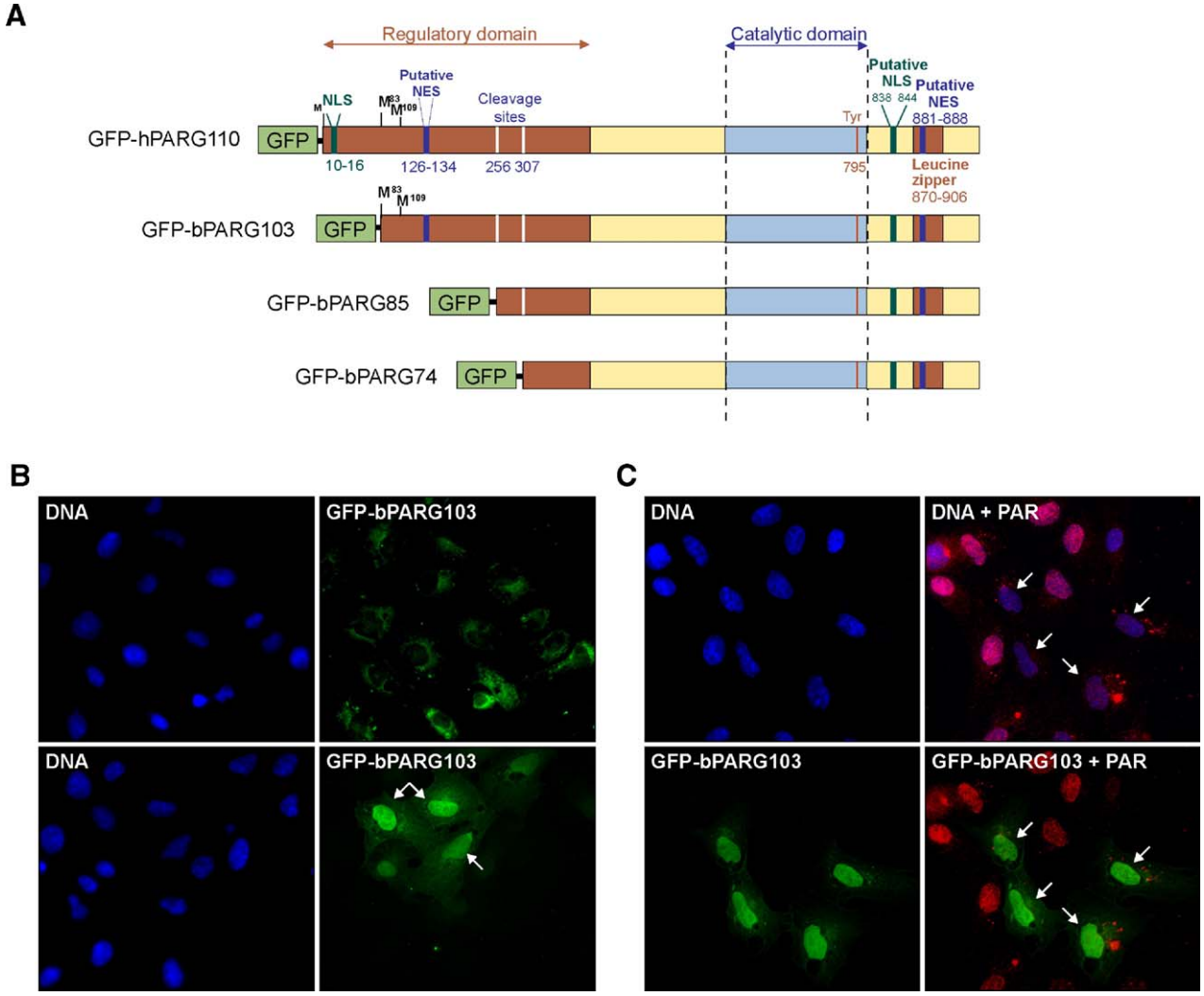

Fig. 1. Dynamic of 103 kDa PARG during radiation-induced DNA damage. (A) Schematic diagram of the GFP-fused PARG proteins used for live cell imaging and representation of their putative structural motifs. Sequence alignments spanning a wide range of organisms revealed that PARG sequences have a large and highly conserved catalytic domain in C-terminus along with a well conserved regulatory domain [19]. In addition, analysis of PARG amino acid sequences from different species identified two potential nuclear export signal (NES), one in the N-terminal half, located at amino acid positions 126–134 and the second at the amino acid position 881–888 near the C-terminal domain. Accordingly, GFP-fused construct were preferred in N-terminus in order to produce active chimeric proteins. (B) SK-N-SH cells were transiently transfected with the fusion constructs and moderately expressing cells were left untreated (top panel) or irradiated with γ-ray (5 Gy) (bottom panel). Following a 4-h recovery period under optimal conditions, cells were fixed with 4% formaldehyde and GFP-hPARG103 cellular localization was observed by fluorescence microscopy. Cells with nuclear translocation are indicated by arrows. DNA was counterstained with Hoechst 33342. (C) SK-N-SK cells expressing GFP-bPARG103 were irradiated (5 Gy), fixed and analysed by indirect immunofluorescence microscopy using anti-PAR 96-10 antibodies (right panel). DNA was stained with Hoechst 33342. Irradiation rapidly stimulates PAR synthesis in untransfected cells, whereas cells expressing GFP-bPARG103 (indicated by arrows) shown a limited PAR accumulation.

unstimulated cells. In response to genotoxic stress, the levels of PAR can increase by 10- to 500-fold [28,30,31] in a fashion that is directly proportional to the number of DNA strand breaks [32,33]. Furthermore, it has been recently reported that during DNA damage, the increased PAR synthesis leads to caspase-independent cell death [3,34] supporting the hypothesis that PAR turnover is essential for cell survival. Accordingly, recent knockout models of PARG in *Drosophila* [35] and mice [20,36,37] revealed that deletion or knockout of the PARG gene results in hypersensitivity to DNA damage-induced cell death and causes profound neurodegeneration. Thus, it is extremely important that both cytoplasmic and nuclear levels of ADP-ribose polymers are tightly controlled in order to prevent PARP-1-induced cell death [11,38,39]. Therefore, it is not surprising that PARG activity has been found to be critical for the prevention of PARP-1 dependent cell death by regulating the intracellular levels of PAR [38,40].

In this paper, we examined the spatiotemporal regulation and dynamics of PARG during radiation-induced DNA damage. Since most of the PAR synthesis following DNA damage occurs in the nucleus and most of the PARG103 isoform, which is more abundant, is in the cytoplasm, we performed experiments to determine whether or not the cytoplasmic PARG103 translocates to the nucleus during or after radiation-induced DNA damage. Using fluorescence recovery after photobleaching (FRAP), we have characterized the intracellular binding and diffusion kinetics of two major PARG isoforms, 103 and 110 kDa, and determined their cellular distribution. We present direct evidence that the PARG110 relocalizes to the cytoplasm during γ-irradiation while cytoplasmic PARG103 and the apoptotic fragments can access to the nucleus.

2. Materials and methods

2.1. Plasmid constructs and mutagenesis

Expression plasmids encoding for green fluorescent protein (GFP) fused with either the 103 kDa bovine PARG isoform (GFP-bPARG-103), the 85 kDa or 74 kDa apoptotic fragments (GFP-bPARG-85, GFP-bPARG-74) were produced according to Bonicalzi et al. [23]. In addition, an expression construct of the full-length 110 kDa human PARG was obtained by cloning a 3.0-kbp *Eco*RI–*Sal*I polymerase chain reaction fragment, amplified from hPARG cDNA (*ATCC* Image Clone 606-4831) with the following primers pairs: h*PARG* forward (5′-GGCGAATTCCATGAATGCGGGCCCCGGCT-3′) and reverse (5′-ACGCGTCGACTCAGGTCCCTGTCCTTTGCC-3′), in frame to the 5′ end of the pEGFP-C1 expression vector (Clontech). After transfection, this construct generates a fusion protein (GFP-hPARG-110) with GFP at the N-terminal end and hPARG at C-terminal end (Fig. 1A). N-terminal GFP fusion proteins have been selected to produce a fully active PARG construct, which could not be obtained when GFP is fused to the C-terminal active domain. Site-directed mutagenesis has been done on this plasmid to change the aspartic acid by alanine (D→A) into the two caspase cleavage sites in order to produce an uncleavable hPARG-110 construct. This mutagenesis was generated with QuickChange™ XL site-directed mutagenesis kit (Stratagene) with primers pairs: h$PARG_{D253A}$ forward (5′-GCAAGTTGTCAGCAAGCTGAGATAGA-TAGATGTGGTGCC-3′) and reverse (5′-GGCACCACATCTATCTCAGC-TATCTCAGCTTGCTGACAACTTGC-3) to mutate the $_{253}$DEID$_{256}$ site in AEID. The mutation of $_{304}$MDVD$_{307}$ site in MDVA was performed using the primers pairs: h$PARG_{D307A}$ forward (5′-CCCGAGTCACCGATGGATGTGGC-TAATCTAAAAATAG-3′) and reverse (5′-CTATTTTTAGAATTAGCCA-CATCCATCGGTGACTCGG-3′). The following plasmids were obtained after mutagenesis: GFP-hPARG-110_{AEID} and GFP-hPARG-$110_{AEID/MDVA}$. All constructs sequences were verified by automated DNA sequencing.

2.2. Cell culture, transfection, and ionizing radiation conditions

Human neuroblastoma SK-N-SH cells obtained from the American Type Culture Collection were grown in Dulbecco's modified Eagle's medium (DMEM) supplemented with 10% fetal bovine serum (FBS), penicillin (100 U/ml) and streptomycin (100 μg/ml). Cells were maintained at 37 °C, under a 5% CO_2 controlled atmosphere in a humidified incubator. For expression of all GFP-fusion proteins, SK-N-SH cells were grown either on coverslips or in 10-cm-diameter culture dish at 60% confluence and transiently transfected with Effecten reagent (Qiagen) according to the manufacturer's protocols. Cells were exposed to a dose of 2 or 5 Gy with a Gammacell-40 γ-ray irradiator (Nordion) depending of experimental procedures. Controls were run in parallel without γ-irradiation. We used molecular markers characteristic of cells bearing DNA double-strand breaks. These markers include nuclear foci of phosphorylated ATM kinase and PAR synthesis.

2.3. Indirect immunofluorescence staining

Transiently transfected cells were fixed 24 h post-transfection with 4.0% paraformaldehyde in phosphate-buffered saline (PBS) (pH 7.5) for 15 min at room temperature. Cells were stained with an appropriate primary antibody diluted in 45-μl aliquots of PBS containing 10% FBS and 1% Triton X-100 for 1 h at room temperature. Coverslips were rinsed with PBS containing 10% FBS and 1% Triton X-100 and washed twice with PBS prior to a 30-min incubation with an appropriate secondary antibody conjugated to a fluorophore. Finally, paraformaldehyde-fixed cells were counterstained with Hoechst 33342 to stain DNA. PAR synthesis was visualized with the rabbit anti-PAR 96-10 antibody and an anti-rabbit Texas-Red conjugated secondary antibody (Jackson Laboratory). Phosphorylation of ATM protein kinase was visualized with a phospho-ATM (Ser1981) (clone 10H11.E12) mouse monoclonal antibody (Cell Signalling) and an anti-mouse Alexa-Fluor 488 secondary antibody (Molecular Probes).

2.4. Fluorescence microscopy analysis

Coverslips labelled as described above were mounted in polyvinyl alcohol (PVA) medium containing antifading agents, sealed and placed on a Nikon TE2000E inverted microscope equipped with an oil immersion 100×1.40 N.A. objective and a Hamamatsu Orca ERS deep cooled CCD camera. For determination of PARG localization, multiple fields were examined to count at least 200 cells. Z-series extending above and below individual nuclei were collected at 500-nm intervals. Images were acquired under identical conditions, ensuring that the maximal signal was not saturated. Images were processed by constrained iterative deconvolution procedure in Priism/IVE 4.0 software [41] by using the enhanced ratio method. Deconvolved images were visualized in Imaris 4.0 (Bitplane). Image brightness/contrast and baseline subtraction were adjusted using Imaris 4.0 (Bitplane) and the measurement of fluorescence intensity and colocalization was performed using MetaMorph 6.0 (Universal Imaging) software. Composite figures of collected images were assembled in Adobe Photoshop.

2.5. Fluorescence recovery after photobleaching (FRAP)

During FRAP experiments, a defined area of a living cell is bleached irreversibly by a high-energy laser pulse. The recovery of the fluorescence signal in the bleached area corresponds to movement of the GFP-fusion protein and is monitored in real-time with low-intensity scanning laser light (0.1%). FRAP analysis was carried out with living SK-N-SH cells grown on coverslips. Cells were transfected with various GFP fusion proteins and mounted on an incubation chamber filled with medium 24 h after transfection. A laser-scanning confocal (Zeiss LSM 510) equipped with a 488-nm laser light and a 40 × 1.3 N.A. objective was used to perform all photobleaching experiments. Fluorescence recovery was monitored over a 16 s period for fast recovery and 30 s for nucleolar recovery. For data analysis, normalization was performed to account for the initial

photobleaching and the smaller amount of photobleaching that occurs during the collection of the individual time points. In the normalized data set presented, 100% recovery represents the theoretical value that the photobleached regions will attain after accounting for the amount of fluorescence lost during the original photobleaching. Details of data normalization have been presented elsewhere [42,43]. Differential interference contrast (DIC) images were also collected to ensure that cells were viable.

2.6. PARG activity gels

Wild-type and transfected SK-N-SH cells were scraped in PBS containing complete protease inhibitor cocktail (Roche Molecular Biochemicals) and an equal volume of 2× sample buffer (100 mM Tris–HCl pH 6.8, 4% SDS, 20% glycerol, 10% β-mercaptoethanol, 0.2% bromophenol blue) supplemented with protease inhibitor cocktail prior to sonication. Samples were neither heated nor frozen before loading. Activity gels were immediately performed as described by Brochu et al. using ^{32}P-automodified PARP-1 as a source of poly(ADP-ribose) [44].

2.7. Subcellular fractionation, SDS-PAGE and western blot analysis

Cellular fractionation was carried out essentially as described by Chi and Lodish [45] and subcellular fractionation was accomplished by differential centrifugation [46]. Cells were resuspended in an hypo-osmotic solution containing 10 mM Tris–HCl pH 7.4, 10 mM NaCl, 1.5 mM $MgCl_2$, 0.1% Triton X-100, 1 mM dithiothreitol, 0.5 mM phenylmethyl sulfonyl fluoride and complete protease inhibitor cocktail. Cells were kept on ice for 15 min and then homogenized in a tight-fitting Dounce homogenizer. Prior to centrifugation, sucrose was added to the homogenate to obtain a final concentration of 250 mM (using a solution containing 2.5 M sucrose, 50 mM Tris–HCl pH 7.4 and 10 mM EDTA) before addition of 140 mM KCl. Whole cell extract (WCE) was centrifuged at 1000×*g* for 10 min to recover nuclei (P1). The supernatant (S1) was clarified at 15,000×*g* for 10 min. The P15 pellet was kept and designed to be the mitochondria-enriched fraction. The supernatant (S15) obtained was again centrifuged at 100,000×*g* for 60 min. The supernatant (S100) was used as cytosolic fraction. Pellets (P1 and P15) were resuspended in a solution containing 250 mM sucrose, 10 mM Tris–HCl pH 7.4, 0.5 mM EDTA and complete protease inhibitor cocktail. Protein concentration was determined by the Bradford assay (BioRad). Proteins were separated in 4–12% linear gradient SDS-PAGE and then electroblotted onto a 0.2 μm nitrocellulose membrane (BioRad). The membranes were probed with anti-GFP (Clonetech), anti-PARP-1 (clone C2-10), anti-PAR 96-10 and anti-actin antibody, followed by the appropriate secondary antibody. Immunoblots were visualized by enhanced chemiluminescence (ECL plus reagent; PerkinElmer) and exposure to X-ray film (Kodak).

2.8. PARG activity assays

PARG activity was measured essentially as described by Jonsson et al. [47]. The different subcellular fractions were prepared as described above. The reaction mixture for the assay contained 50 mM potassium phosphate pH 7.5, 50 mM KCl, 100 μg/ml bovine serum albumin, 10 mM β-mercaptoethanol, 0.1 mM PMSF, 10μM [^{32}P]-labelled PAR. The reaction was started by the addition of the cell extracts and stopped after 10 min by the addition of SDS at a 0.1% final concentration. An aliquot of each reaction was applied on polyethyleneimine-cellulose TLC plate. The plate was first developed at room temperature in methanol, dried, and then developed in 0.3 M LiCl, 0.9 N acetic acid. The TLC plate was electronically autoradiographed on Instant Image Analyzer (Packard Instrument Company) to determine the amount of radioactivity in each spot. The amounts of radioactivity found in the ADP-ribose spot and the origin were used to calculate PARG-specific activity. One unit of PARG is defined as the amount of enzyme required to release 1 nmol of ADP-ribose per min at 37 °C under assay conditions.

2.9. Data analysis

Fluorescence recovery values were exported to Microsoft Excel to calculate the FRAP curves with correction for total fluorescence loss. These corrected values were copied to SigmaPlot 8.0 software (SYSTAT Software Inc.) for non-linear regression analysis using the single exponential association curve fitting equation with <95% confidence. All values are expressed as mean±S.E.M. Statistical significance of difference between two groups was tested using Student *t*-test. *P* values less than 0.05 were considered to be significant. When data sets were compared, identical conditions were used in photobleaching experiments including the number of cells, the area of the photobleach region and the time course of imaging at low laser power (0.1%).

3. Results

3.1. Dynamics of the cytoplasmic PARG103 isoform

We first investigated the cellular distribution of major 103 kDa bovine PARG isoform (bPARG103) during radiation-induced DNA damage using GFP fusion protein and live cell imaging. It is now well accepted that PARG103 enzyme is cytoplasmic [18,23] and represents the most abundant PARG form in both quantity and activity. To study the distribution of PARG103, we used transiently transfected human SK-N-SH neuroblastoma cell line with GFP-bPARG103 24 h prior to γ-irradiation. The construction of an N-terminal fusion of PARG with enhanced GFP used for FRAP analysis in living cells is an elegant approach since it allows the expression of a fully active enzyme, which was not obtained when the GFP is fused to the C-terminal catalytic domain. We first established that the different GFP-PARG fusion proteins behave like their wild type counterparts in terms of activity and cellular localization. Although the fusion protein behaves like its endogenous counterpart, we cannot rule out that there is a modest reduction in the binding affinity of the eGFP tagged PARG. Accordingly, we validated that GFP-bPARG103 is distributed mostly in the cytoplasm of untreated neuroblastoma cells. In addition, we observed that the GFP-bPARG103 translocates into the nucleus in the presence of ionizing radiation (Figs. 1B–C). This is, to our knowledge, the first instance where nuclear translocation of the PARG103 is observed in living cells after DNA damage induction, although it has previously been shown that GFP-bPARG103 would accumulate into the nucleus following leptomycin B treatment [23]. Fluorescence microscopy analysis reveals that all four transfected cells shown in Fig. 1C exhibit a lower PAR accumulation compared to untransfected ones. This is consistent with previously reported overexpression experiments which suggest that the transition of bPARG103 isoform from cytoplasm to nucleus might regulate PAR catabolism [11,23].

We next analyzed whether γ-irradiation affects the kinetics of PARG103 in various cellular compartments. Accordingly, we performed FRAP experiments on cells overexpressing GFP-bPARG103. We thus irreversibly bleached the fluorescence of GFP-bPARG103 in a small region of the nucleus or cytoplasm and subsequently recorded the recovery of fluorescence over a period of 16 s [43]. The kinetics of recovery was measured at specific time points (1, 4 and 24 h) following γ-irradiation and corresponds to the mobility of the labelled GFP-PARG103 proteins within the cell compartments. Using this approach, we observed differences in the recovery after photobleaching between the nuclear and cytoplasmic sub-populations (Fig. 2).

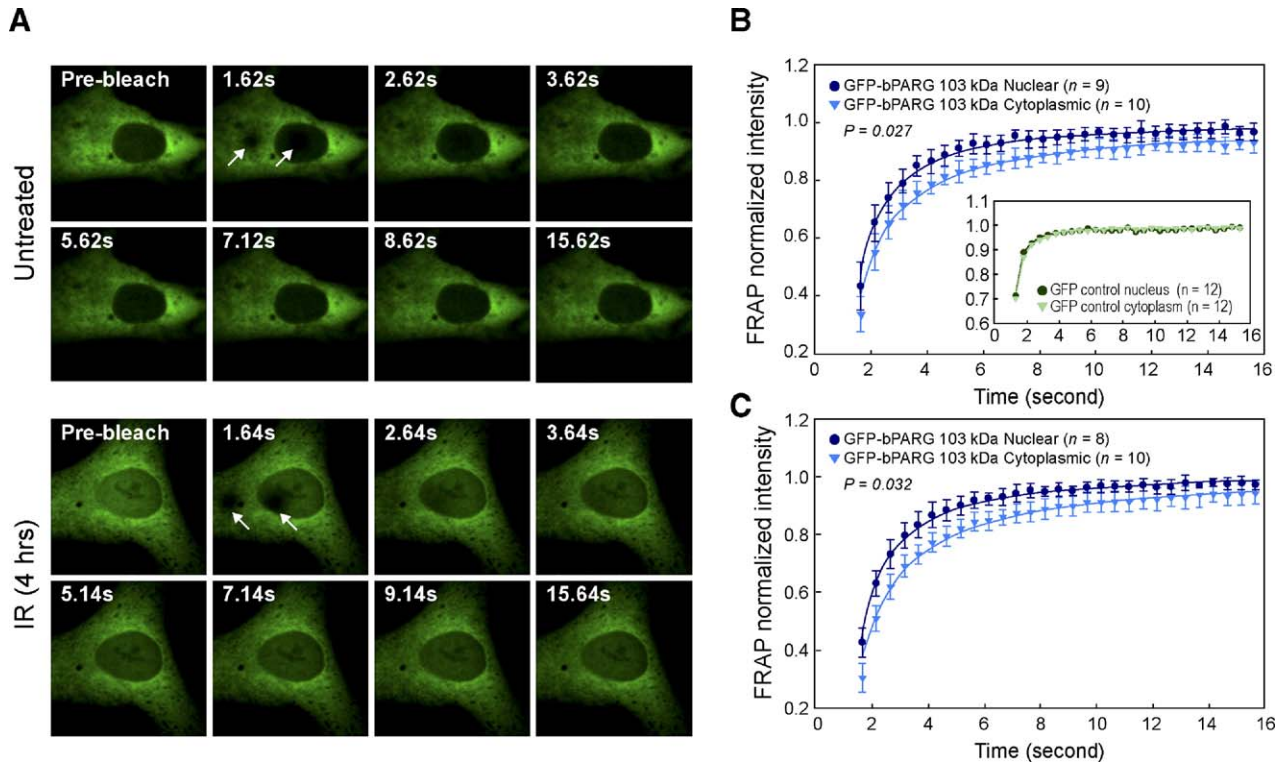

Fig. 2. Fluorescence recovery after photobleaching analyses of nuclear and cytoplasmic GFP-bPARG103 isoform. Transiently expressed GFP-bPARG103 constructs in live SK-N-SH cells were subjected to quantitative FRAP analysis. (A) The upper panel shows the time-lapse images collection of GFP-bPARG103 recovery after photobleaching in untreated cells. The bottom panel shows FRAP images of GFP-bPARG103 expressing cell 4 h after irradiation (2 Gy). Time in seconds is shown at the top of each panel. The nuclear and cytoplasmic region where FRAP was performed is indicated by arrows. (B–C) For quantitative analysis, fluorescence recovery in the bleached area and intensities in different cytoplasmic and nuclear regions as well as the background signal were quantified with minimal laser power. Data obtained for recovery were corrected for the background intensity and loss of total fluorescence. The insert presents data obtained from fluorescence recovery of GFP control experiments. The plot shows normalized mean values of fluorescence intensity versus time in seconds after photobleaching. The mobility of GFP-bPARG103 in cytoplasmic and nuclear compartments was compared (B) before and (C) 4 h after γ-irradiation (2 Gy). *P* values calculated using the Student's *t* test indicate the significance of the difference in recovery time between nuclear and cytoplasmic pool of GFP-bPARG103.

The nucleoplasmic kinetics of recovery for the GFP-bPARG103 protein is significantly faster than it was in the cytoplasm. In undamaged cells, nuclear and cytoplasmic fluorescence recovery of GFP-bPARG103 was completed in 7.12 s and 12.12 s, respectively. Despite being catalytically active, γ-irradiation does not affect the recovery time of either nuclear or cytoplasmic population of PARG103 (Figs. 2B–C). Accordingly, we noticed that 4 h following γ-irradiation the fluorescence recovery of nuclear and cytoplasmic GFP-bPARG103 was completed in 7.65 s and 11.65 s, respectively.

3.2. Nuclear to cytoplasm translocation of PARG110 following genotoxic stress

To further investigate the nuclear localization of full-length PARG, we used cells transfected with GFP-hPARG110 vector and performed biochemical measurements. First, we demonstrate that the level of poly(ADP-ribosyl)ation in neuroblastoma cells overexpressing GFP-hPARG110 was significantly reduced following γ-irradiation relative to control cells, consistent with an enzymatically active GFP-hPARG110 in transfected cells (Figs. 3A–B). Additionally, the majority of endogenous PARG activity was found in the cytoplasm, whereas cells overexpressing GFP-hPARG110 have an increased nuclear PARG activity (Fig. 3C). Other groups also report that the PARG cytoplasmic isoforms predominate within cells [18,22,23].

Using fluorescence microscopy, we confirm the previously observed nuclear localization of the GFP-tagged full-length human PARG110 in untreated mammalian cells (Fig. 4) [18,22,25]. Somewhat unexpectedly, fluorescence microscopy analysis revealed that the subcellular distribution of GFP-hPARG110 changes dramatically during γ-irradiation. We observed that the GFP-hPARG110 relocalizes to the cytoplasm as rapidly as 1 h after induction of DNA damage by γ-irradiation (Fig. 4). Likewise, it has been reported previously that during mitosis most of the GFP-hPARG110 protein does not associate with chromosomes [22]. We ascertain that the 5 Gy dose of γ-irradiation used in our experiments induces significant DNA double-strand breaks and results in massive PAR synthesis (Fig. 5A). Thereafter, we used an activity gel to visualize the full-length GFP-hPARG110 protein activity before and after DNA damage induction; the GFP-hPARG110 was detected at ~140 kDa (Fig. 5B).

To ensure that this nuclear to cytoplasmic relocation is achieved by the full-length GFP-tagged hPARG110 and does not represent the behaviour of caspase-3 cleaved GFP-fragment, we engineered constructs where the two caspase cleavage sites DEID and MDVD were mutated to uncleavable

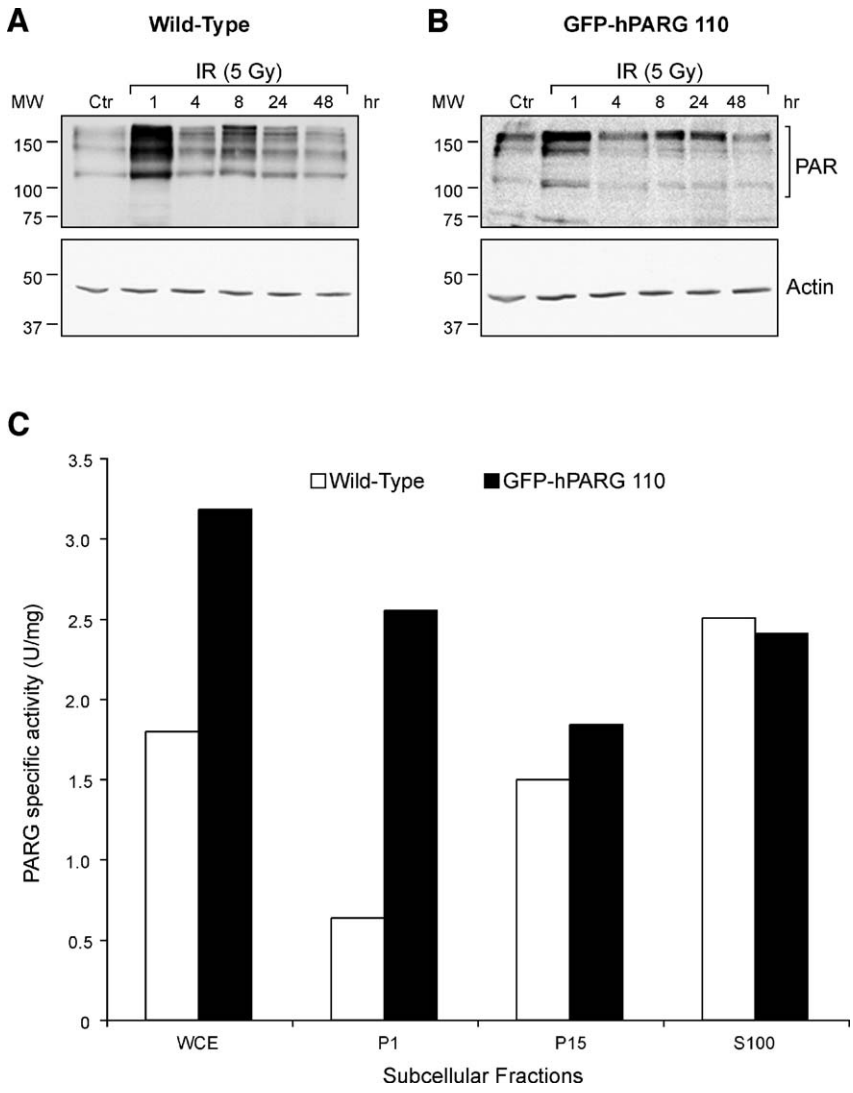

Fig. 3. Activity of endogenous and GFP-hPARG110 expressing neuroblastoma cells. SK-N-SH cells were treated with γ-irradiation (5 Gy) or left untreated. Total extracts from (A) wild-type and (B) GFP-hPARG110 expressing cells were prepared and immunoblotted with anti-PAR antibodies. Actin blot were shown as a loading control. PAR stimulation is less abundant in cells overexpressing hPARG110. (C) Histogram displaying PARG-specific activity in different subcellular fractions of wild-type cells and GFP-PARG110 overexpressing cells. SK-N-SH cells were fractionated by differential centrifugation as described in Materials and methods. Extract from whole cell extract (WCE), pellets (P1, P15) and supernatant (S100) were analysed for PARG using the TLC assay. Data from a representative experiment is shown.

hPARG110 isoforms. Thus, for the first time, we report that the $hPARG110_{AEID/MDVA}$ could not be cleaved by caspase-3 following DNA damage, whereas the wild-type GFP-hPARG110 as well as PARP-1 were effectively cleaved after this genotoxic stress (Figs. 5C–E). According to the PARG activity gel presented in Fig. 5B, none of the GFP-PARG110 constructs was cleaved by caspase-3 before or 1 h after radiation-induced DNA damage. We show that the two uncleavable GFP-hPARG110 constructs translocate from the nucleus to the cytoplasm in a manner that is quantitatively indistinguishable from wild-type hPARG110 (Fig. 4).

3.3. Nuclear PARG110 associates with nucleoli

When we examined the nuclear fluorescence pattern of GFP-hPARG110 in living cells, we observed a slight enrichment within the nucleolus (Fig. 6). To confirm that this localization overlapped with known nucleolar proteins, we co-transfected SK-N-SH neuroblastoma cells expressing GFP-hPARG110 with a nucleolin-DsRed vector. When we compared the nucleolin-DsRed and GFP-hPARG110 we found that a sub-population of nuclear hPARG110 colocalizes with nucleolin in vivo (Fig. 6A). Based on our observation of the nucleolar accumulation of GFP-hPARG110, we wanted to investigate whether this nucleolar pool is in a dynamic equilibrium with GFP-hPARG110 in the nucleoplasm. FRAP experiments show that GFP-hPARG110 can return into a bleached area defining the nucleolus (Fig. 6B) and the nucleolar pool of GFP-hPARG110 was replenished in about 22 s. Thus, hPARG110 is dynamically associated with nucleolar components. This result is consistent with the recent observation that GFP-hPARG110 binds to nucleolar proteins [25]. Surprisingly,

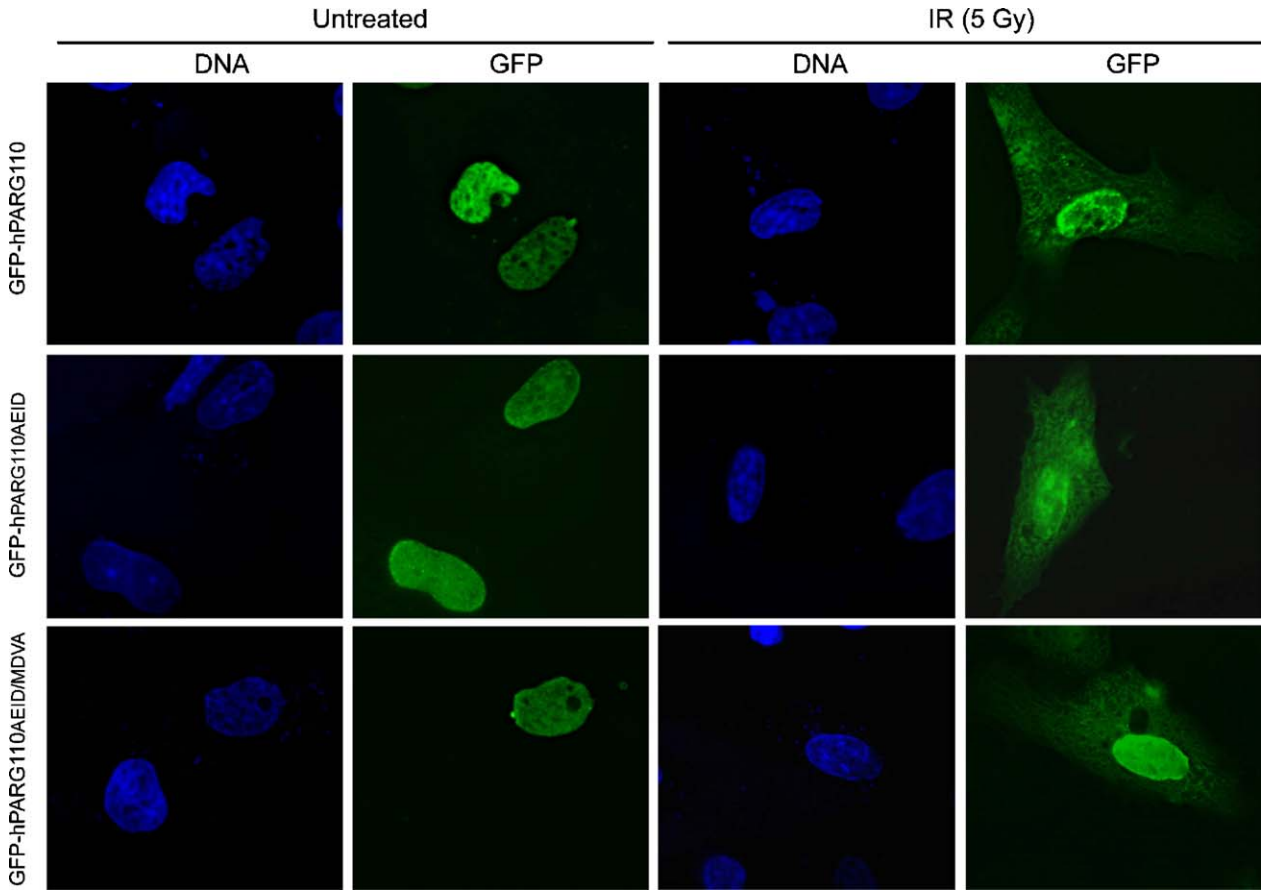

Fig. 4. Nuclear to cytoplasmic translocation of 110 kDa PARG after DNA damage. SK-N-SH cells were transiently transfected with the fusion constructs and moderately expressing cells were left untreated or irradiated with γ-ray (5 Gy). Following a 1-h recovery period under optimal conditions, cells were fixed with 4% formaldehyde and GFP-hPARG110 cellular localization was observed by fluorescence microscopy. DNA was counterstained with Hoechst 33342. Z-series extending above and below individual nuclei were collected at 500-nm intervals. Selected focal plan from deconvolution images are presented for GFP fluorescence (green) along with nuclear DNA staining (blue). For the determination of GFP-hPARG110 localization after DNA damage, multiple fields were examined to count at least 200 cells for each constructs. GFP-fusion proteins are indicated on the right.

nucleolar localization is sometimes also observed for apoptotic fragments when located in the nucleus (Figs. 7B and C).

3.4. Localization and regulation of PARG apoptotic fragments during radiation-induced DNA damage

In previous studies, Affar and coworkers found that all forms of endogenous PARG (110, 103 and 99 kDa) were cleaved in human cells during DNA damage-induced apoptosis [21]. Caspase cleavage sites were identified at amino acid position 256 (DEID) and 307 (MDVD) of the human PARG sequence. It was further demonstrated that PARG cleavage by caspase-3 generated two C-terminal fragments of 85 and 74 kDa that retained full PARG enzymatic activity [21,23]. Because the two apoptotic fragments remain active, it was important to define their cellular distribution and dynamics in order to better understand their relative roles. To determine whether or not PARG85 and PARG74 apoptotic fragments are regulated differently, SK-N-SH neuroblastoma cells were transiently transfected with GFP-bPARG85 or GFP-bPARG74 and, after allowing time for expression, time-lapse microscopy and photobleaching studies were examined over a 24-h period. In untreated cells, all GFP-fusion proteins colocalized with their endogenous counterparts (Fig. 7 and [23]). Moreover, we noticed that a larger number of cells expressing GFP-bPARG85 or 74 exhibited nearly equal distribution of GFP fluorescence throughout the cell at 4 and 24 h after γ-irradiation (Fig. 7). The time lapse fluorescence microscopy observations reflect the steady-state equilibrium of the nuclear import and nuclear export processes and show that all PARG isoforms, including apoptotic fragments, are in continuous flux between cytoplasm and nucleus. Upon stimulation by γ-irradiation, we observed that the apoptotic fragments PARG85 and PARG74 also translocate from the cytoplasm into the nucleus of living cells. Four hours after DNA damage induction, we observed a nuclear fluorescence from GFP-bPARG85 and 74 overexpressing cells similar to what we observed in cells overexpressing GFP-bPARG103 (Fig. 7). This implies that nuclear accumulation of the apoptotic fragments following radiation-induced DNA damage could also play a prominent role in regulation of PAR catabolism.

This information allowed us to follow the behaviour of GFP-tagged apoptotic fragments by FRAP analysis following γ-irradiation. Although the subcellular distribution was altered,

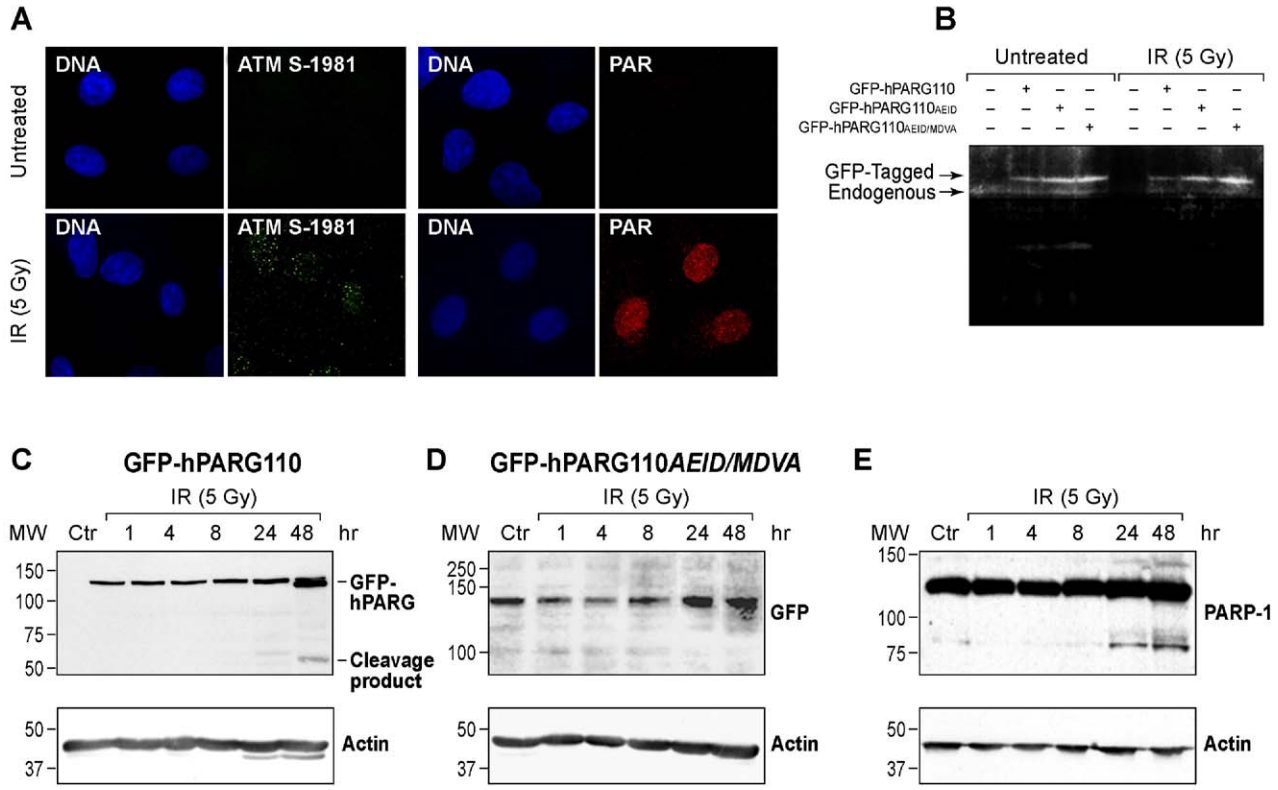

Fig. 5. Irradiation activates early PAR synthesis followed by late hPARG110 and PARP-1 cleavage. (A) SK-N-SK cells were irradiated (5 Gy), fixed and analysed by indirect immunofluorescence microscopy using anti-PAR 96-10 antibodies (right panel) and anti-phospo-ATM ser 1981 antibodies (left panel). DNA was stained with Hoechst 33342. Irradiation rapidly stimulates PAR synthesis and ATM Ser-1981 phosphorylation in neuroblastoma cells. (B) PARG activity gel of SK-N-SH cells following treatment with γ-irradiation (5 Gy). Lysates of untransfected SK-N-SH cells or cells expressing GFP-hPARG110 and each of the 2 uncleavable mutated proteins were prepared and enzymatic activity was detected by performing activity gel as describe in Materials and methods. GFP-hPARG110 construct are active before and after DNA damage induction and they were not cleaved at 1 h after irradiation. SK-N-SH cells expressing either (C) GFP-hPARG110 or (D) GFP-hPARG$_{AEID/MDVA}$ were treated with γ-irradiation (5 Gy) or left untreated. Total extracts were prepared and immunoblotted with anti-GFP antibodies and anti-actin. (E) Total extracts prepared from wild-type neuroblastoma cells and immunoblotted with anti-PARP-1 and anti-actin antibodies. PARP-1 cleavage was used as indicator of apoptosis induction. GFP-hPARG110 is efficiently cleaved as well as PARP-1 in radiation induced DNA damage. The uncleavable mutant remains intact under the same conditions.

we observed no difference in the recovery rate between GFP-bPARG103 and the apoptotic fragments (Supplementary Fig. S1). As we presented for GFP-bPARG103, the fluorescence recovery of both GFP-bPARG85 and 74 was complete by approximately 8 s for nuclear population and 12 s for cytoplasmic pool. Taken together, these results indicate that caspase-3 cleavage of PARG does not affect either the activity or mobility of PARG. Therefore, there is no evidence that, once generated, the apoptotic fragments are not participating in PAR metabolism.

4. Discussion

The synthesis and rapid turnover of ADP-ribose polymers is an immediate cellular response to DNA damage [7], but, in contrast to the well-characterized role of PARP-1, the behaviour of PARG in the response to DNA damage has not been extensively studied. In this report, we employed live cell imaging to define the dynamic localization and relocation of two major PARG isoforms, 103 and 110 kDa, following radiation-induced DNA damage. Earlier studies using immunocytochemistry or expression of GFP-fused PARG have previously revealed nuclear accumulation upon leptomycin B treatment [23] and the steady-state distribution of PARG between nucleus and cytoplasm [18,22,23,48]. These properties are dictated by the relative rates of nuclear import and export. Our results reveal that the subcellular distribution of PARG is more dynamic than previously thought.

In this study, we demonstrate that even though GFP-bPARG103 is predominantly localized in the cytoplasm in absence of genotoxic stress, it rapidly shuttles between the cytoplasm and the nucleus following DNA damage. It is important to note that even if PARG103 lacks the entire exon 1 encoded NLS motif, it was still able to be imported into the nucleus when DNA damage is present. We cannot exclude that the putative NLS identified in C-terminal catalytic domain (Fig. 1A) could account for its nuclear localization or that nuclear import could be mediated by a binding partner [11,23]. In addition to the remarkable change in localization (Figs. 1B–C), we examined whether the induction of DNA damage by γ-irradiation altered the mobility of GFP-bPARG103 within either compartment. This issue is important because such a change would be a reflection of a change in the protein–protein or enzyme–substrate interactions of PARG following genotoxic

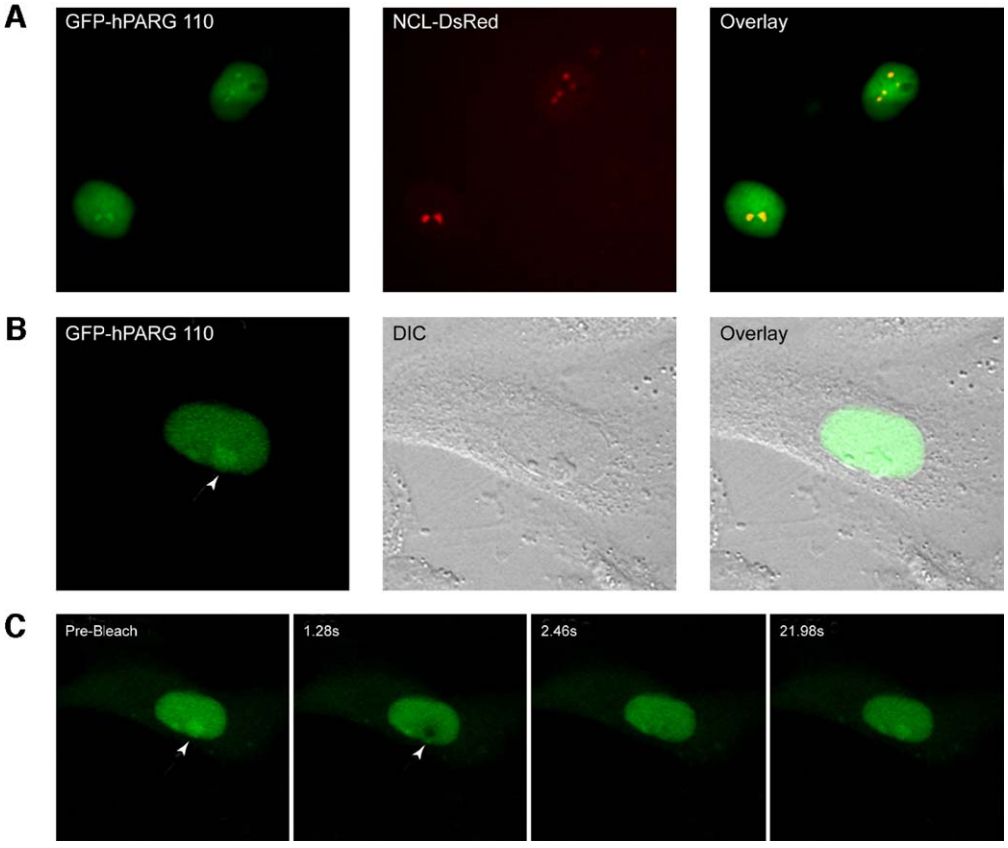

Fig. 6. Nuclear 110 kDa full-length PARG can be associated with nucleoli. (A) SK-N-SH cells cotransfected with nucleolin-DsRed and GFP-hPARG110 were imaged 24 h after transfection. Fluorescent images were captured in living cells overexpressing both construct. The overlay of GFP-hPARG110 fluorescence and the nucleolin-DsRed shows colocalization of these proteins in nucleoli. (B) Live-cell fluorescent patterns of cells transfected with GFP-hPARG110 alone. The nucleolar structures are indicated by arrows. (C) Transiently transfected SK-N-SH cells expressing GFP-hPARG110 were bleached in a small area of an entire nucleolus (indicated by an arrow) and nucleolar import then visualized over 30 s by low intensity laser-scanning multi-photon microscopy to assess the return of fluorescence. Recovery of GFP-hPARG110 in nucleolus is seen in less than 22 s.

stress. Thus, we performed FRAP experiments on living neuroblastoma to study the mechanism responsible for the change in GFP-bPARG103 subcellular distribution. An underlying feature is that PARG displays very fast kinetics and has a transient localization in the nucleus. Because the GFP-PARG fusion proteins used in our experiments retain the capacity to degrade PAR polymers, our results imply that the GFP-bPARG103 has the potential to rapidly reach sites of massive PAR synthesis that are triggered by signals elicited after DNA damage (Fig. 1C). Another important conclusion is that the nuclear fluorescence recovery time of the PARG103 isoform is within the same range as PAR turnover observed after DNA damage [30,49]; both of them are completed in less than 30 s.

However, we found that the kinetics of GFP-bPARG103 is not significantly influenced by genotoxic stress, supporting the hypothesis that the nucleocytoplasmic shuttling dynamics, rather than protein–protein interactions, is altered by DNA damage. Consequently, this alteration of the nucleocytoplasmic shuttling dynamics is expected to change the relative amount of enzymatically active PARG103 isoform between the nuclear and cytoplasmic compartments. We also found that the recovery of GFP alone was significantly faster than fusion proteins independently of their cellular distribution (Fig. 2B, insert). Although the mobility of fusion proteins is significantly lower than GFP alone (Fig. 2B), we found that protein immobilization is not responsible for the retention of PARG103 in the cytoplasm since PARG can diffuse throughout intracellular compartments. None of the results presented here support a hypothesis that PARG103 is restricted to or tightly associated with an organelle. Rather, the results on GFP-bPARG103 revealed rapid recovery that is consistent with a soluble enzyme undergoing very transient reversible binding to very large macromolecules of cellular structures. Therefore, we propose that the regulated cytoplasmic and nuclear trafficking plays a critical role in determining the overall distribution of PARG103 isoform in untreated cells and upon radiation-induced DNA damage. The pathway involved in the transport of PARG is mostly unknown, but we speculate that γ-irradiation trigger a change from a tight and controlled nucleocytoplasmic shuttling to a leakier nuclear envelope allowing rapid exchange of PARG between the two compartments. Clearly, more work is required to elucidate the molecular mechanisms that regulate the equilibrium between nuclear import and nuclear export following γ-irradiation.

Consistent with a potential role at an early step of radiation-induced damage [50], we demonstrate that, following γ-

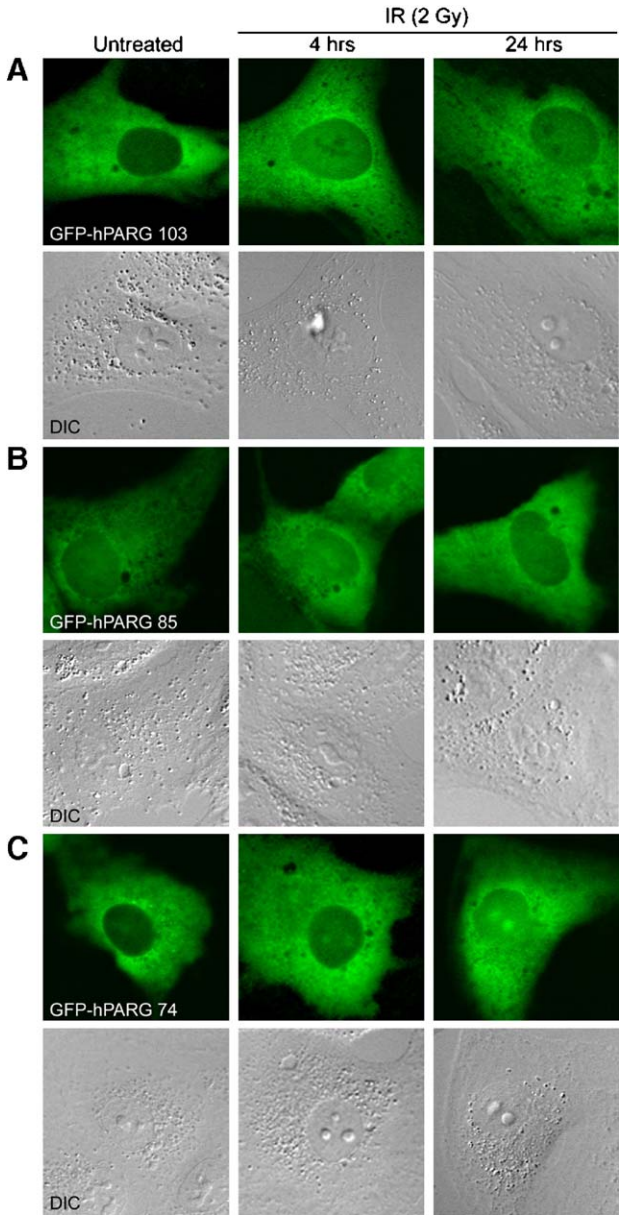

Fig. 7. Cellular localization of the 103 kDa PARG and the two apoptotic fragments following radiation-induced DNA damage. Fluorescence microscope images of living SK-N-SH cells transiently transfected with GFP-bPARG103 isoform (A), as well as apoptotic fragments GFP-bPARG85 (B), and GFP-bPARG74 (C). DNA damage were induced in SK-N-SH with γ-irradiation at a 2-Gy dose and imaged at specific time points by multi-photon fluorescence microscopy. DIC images were also collected to monitor cell viability. We observe more than 100 cells for each condition and representative images were shown. The regulation of subcellular localization following radiation-induced DNA damage was the same for these three isoforms.

irradiation, the nuclear hPARG110 relocalizes in the cytoplasm (Fig. 4). We used several uncleavable hPARG constructs to ensure that the fluorescence of GFP-hPARG110 would reflect, as closely as possible, the cellular distribution of the full-length hPARG110 rather than the caspase-3 cleavage products. Thus, we verified that relocation of hPARG110 following γ-irradiation is not the result of caspase-3 cleavage since the uncleavable mutants redistribute in a manner identical to hPARG110 (Fig. 4). Collectively, our findings support the hypothesis that under conditions of genotoxic stress, the translocation of nuclear hPARG110 to cytoplasm promotes nuclear PAR accumulation. Consistent with this notion is the observation that *N*-methyl-*N*′-nitro-*N*-nitrosoguanidine (MNNG) treatment resulted in a decrease of nuclear PARG activity [18]. Our results provide the first evidence that the transient decrease in PARG activity can be determined by nucleocytoplasmic translocation of PARG110 isoform and is not simply the result of caspase 3-mediated cleavage. This remarkable observation provides *in vivo* evidence that PARG subcellular distribution may be used to maintain an appropriate PAR threshold under normal and pathological conditions.

We have shown that the majority of hPARG110 is located in the nucleoplasm of undamaged neuroblastoma SK-N-SH cells (Fig. 4), and that the enzyme also enriches in the nucleolus (Fig. 6). Interestingly, a significant subnuclear population of PARP-1 and PARP-2 is also located in the nucleolus [51] and a recent proteomics analysis of the human nucleolus confirmed the nucleolar localization of PARP-1 [52]. The interdependency between nucleolar accumulation of PARPs and poly(ADP-ribosyl)ation of nucleolar proteins has been described in the past [53,54]. Indeed, it has been shown that PAR synthesis induced by alkylating agents is less efficient in the nucleolus than in the nucleoplasm [51]. Thus, our observation that the association of hPARG110 with the nucleolar region might involve the sequestration of the active enzyme would explain the lower steady-state level of poly(ADP-ribosyl)ation previously observed in nucleolus. Although we have identified interactions between PARG and other nucleolar proteins [25], we cannot completely exclude the possibility that the hPARG110 accumulation in the nucleolus is the result of an interaction with either PARP-1 or PARP-2. Consequently, the regulation of nucleolar localization of PARG110 by protein–protein interactions is a tempting hypothesis given that nucleolar PARG has been demonstrated to be a member of a ribonucleoprotein complex [25]. In that case, the nucleolar accumulation of GFP-PARG110 can be explained by a longer retention time of individual GFP-PARG110 complexes in these structures or by a higher concentration of interacting proteins or a combination of both.

Because PARG is cleaved by caspase 3 into catalytically active C-terminal fragments, it was important in our study to define the properties of these isoforms as well. In particular, we wanted to determine whether or not the PARG apoptotic fragments will respond to a damage-induced signal in a manner similar to the uncleaved isoform. We found that caspase-3 cleavage does not affect its dynamic behaviour or subcellular localization. Photobleaching revealed that the two apoptotic fragments move freely and could thus be also engaged in the regulation of PARG metabolism once they are generated.

PARP-1 and poly(ADP-ribosyl)ation play a prominent role in cell death in a number of experimental models [55] suggesting that PARG will be able to relocate to nucleus not only following γ-irradiation but also in MNNG-induced toxicity and NMDA excitotoxicity. Given these possibilities, we assumed that the effect of PARG110 depletion in mice will

be less important than a total ablation of PARG activity because other PARG remains active and can reach the nucleus. Our results strongly support the idea that residual PARG activity observed in mice lacking PARG110 is sufficient to hydrolyze the nuclear PAR and this observation explains why the disruption of the nuclear PARG110 gene is not lethal for the mouse [36]. Consistent with an essentially cellular role for PARG activity, recent findings demonstrated that the complete knockout of PARG is lethal in mouse. This is because the uncontrolled PAR accumulation rapidly leads to the induction of apoptosis in the absence of cellular PARG activity [20,56]. It is reasonable to expect that the control of PARG activity is important in several pathological conditions that involve induction of DNA-strand breaks.

Acknowledgements

We want to thank Veronique Bouchard and Dr. Masahiko Sato for kindly providing the nucleolin-DsRed construct. We also thank Danièle Poirier and Marie-Eve Bonicalzi for critical reading of the manuscript. Dr. Guy G. Poirier holds a Canada Research Chair in Proteomics. This work was supported by the Canadian Institutes of Health Research (CIHR).

Appendix A. Supplementary data

Supplementary data associated with this article can be found in the online version at doi:10.1016/j.bbamcr.2005.11.015.

References

[1] V.J. Bouchard, M. Rouleau, G.G. Poirier, PARP-1, a determinant of cell survival in response to DNA damage, Exp. Hematol. 31 (2003) 446–454.
[2] A. Ivana Scovassi, M. Diederich, Modulation of poly(ADP-ribosylation) in apoptotic cells, Biochem. Pharmacol. 68 (2004) 1041–1047.
[3] S.W. Yu, H. Wang, T.M. Dawson, V.L. Dawson, Poly(ADP-ribose) polymerase-1 and apoptosis inducing factor in neurotoxicity, Neurobiol. Dis. 14 (2003) 303–317.
[4] M.Y. Kim, S. Mauro, N. Gevry, J.T. Lis, W.L. Kraus, NAD+-dependent modulation of chromatin structure and transcription by nucleosome binding properties of PARP-1, Cell 119 (2004) 803–814.
[5] V. Pirrotta, The ways of PARP, Cell 119 (2004) 735–736.
[6] M.L. Meyer-Ficca, R.G. Meyer, E.L. Jacobson, M.K. Jacobson, Poly (ADP-ribose) polymerases: managing genome stability, Int. J. Biochem. Cell Biol. 37 (2005) 920–926.
[7] D. D'Amours, S. Desnoyers, I. D'Silva, G.G. Poirier, Poly(ADP-ribosyl) ation reactions in the regulation of nuclear functions, Biochem. J. 342 (1999) 249–268.
[8] J.C. Ame, V. Rolli, V. Schreiber, C. Niedergang, F. Apiou, P. Decker, S. Muller, T. Hoger, J. Menissier-de Murcia, G. de Murcia, PARP-2, A novel mammalian DNA damage-dependent poly(ADP-ribose) polymerase, J. Biol. Chem. 274 (1999) 17860–17868.
[9] V. Schreiber, J.C. Ame, P. Dolle, I. Schultz, B. Rinaldi, V. Fraulob, J. Menissier-de Murcia, G. de Murcia, Poly(ADP-ribose) polymerase-2 (PARP-2) is required for efficient base excision DNA repair in association with PARP-1 and XRCC1, J. Biol. Chem. 277 (2002) 23028–23036.
[10] J.C. Ame, C. Spenlehauer, G. de Murcia, The PARP superfamily, Bioessays 26 (2004) 882–893.
[11] M.E. Bonicalzi, J.F. Haince, A. Droit, G.G. Poirier, Regulation of poly (ADP-ribose) metabolism by poly(ADP-ribose) glycohydrolase: where and when? Cell Mol. Life Sci. 62 (2005) 739–750.
[12] W. Lin, J.C. Ame, N. Aboul-Ela, E.L. Jacobson, M.K. Jacobson, Isolation and characterization of the cDNA encoding bovine poly(ADP-ribose) glycohydrolase, J. Biol. Chem. 272 (1997) 11895–11901.
[13] J.C. Ame, F. Apiou, E.L. Jacobson, M.K. Jacobson, Assignment of the poly(ADP-ribose) glycohydrolase gene (PARG) to human chromosome 10q11.23 and mouse chromosome 14B by in situ hybridization, Cytogenet. Cell Genet. 85 (1999) 269–270.
[14] E. Winstall, E.B. Affar, R. Shah, S. Bourassa, A.I. Scovassi, G.G. Poirier, Poly(ADP-ribose) glycohydrolase is present and active in mammalian cells as a 110-kDa protein, Exp. Cell Res. 246 (1999) 395–398.
[15] S. Panda, G.G. Poirier, S.A. Kay, tej defines a role for poly(ADP-ribosyl) ation in establishing period length of the Arabidopsis circadian oscillator, Dev. Cell 3 (2002) 51–61.
[16] T. Shimokawa, M. Masutani, S. Nagasawa, T. Nozaki, N. Ikota, Y. Aoki, H. Nakagama, T. Sugimura, Isolation and cloning of rat poly(ADP-ribose) glycohydrolase: presence of a potential nuclear export signal conserved in mammalian orthologs, J. Biochem. (Tokyo) 126 (1999) 748–755.
[17] R.G. Meyer, M.L. Meyer-Ficca, E.L. Jacobson, M.K. Jacobson, Human poly(ADP-ribose) glycohydrolase (PARG) gene and the common promoter sequence it shares with inner mitochondrial membrane translocase 23 (TIM23), Gene 314 (2003) 181–190.
[18] M.L. Meyer-Ficca, R.G. Meyer, D.L. Coyle, E.L. Jacobson, M.K. Jacobson, Human poly(ADP-ribose) glycohydrolase is expressed in alternative splice variants yielding isoforms that localize to different cell compartments, Exp. Cell Res. 297 (2004) 521–532.
[19] C.N. Patel, D.W. Koh, M.K. Jacobson, M.A. Oliveira, Identification of three critical acidic residues of poly(ADP-ribose) glycohydrolase involved in catalysis: determining the PARG catalytic domain, Biochem. J. 388 (2005) 493–500.
[20] D.W. Koh, A.M. Lawler, M.F. Poitras, M. Sasaki, S. Wattler, M.C. Nehls, T. Stoger, G.G. Poirier, V.L. Dawson, T.M. Dawson, Failure to degrade poly(ADP-ribose) causes increased sensitivity to cytotoxicity and early embryonic lethality, Proc. Natl. Acad. Sci. U. S. A. 101 (2004) 17699–17704.
[21] E.B. Affar, M. Germain, E. Winstall, M. Vodenicharov, R.G. Shah, G.S. Salvesen, G.G. Poirier, Caspase-3-mediated processing of poly(ADP-ribose) glycohydrolase during apoptosis, J. Biol. Chem. 276 (2001) 2935–2942.
[22] S. Ohashi, M. Kanai, S. Hanai, F. Uchiumi, H. Maruta, S. Tanuma, M. Miwa, Subcellular localization of poly(ADP-ribose) glycohydrolase in mammalian cells, Biochem. Biophys. Res. Commun. 307 (2003) 915–921.
[23] M.E. Bonicalzi, M. Vodenicharov, M. Coulombe, J.P. Gagne, G.G. Poirier, Alteration of poly(ADP-ribose) glycohydrolase nucleocytoplasmic shuttling characteristics upon cleavage by apoptotic proteases, Biol. Cell 95 (2003) 635–644.
[24] J.C. Ame, E.L. Jacobson, M.K. Jacobson, Molecular heterogeneity and regulation of poly(ADP-ribose) glycohydrolase, Mol. Cell. Biochem. 193 (1999) 75–81.
[25] J.P. Gagné, M.-E. Bonicalzi, P. Gagné, M.-E. Ouellet, M.J. Hendzel, G.G. Poirier, Poly(ADP-ribose) glycohydrolase is a component of the FMRP-associated messenger ribonucleoparticles, Biochem. J. 392 (2005) 499–509.
[26] A.M. Ferro, N.J. Oppenheimer, Structure of a poly (adenosine diphosphoribose) monomer: 2′-(5″-hosphoribosyl)-5′-adenosine monophosphate, Proc. Natl. Acad. Sci. U. S. A. 75 (1978) 809–813.
[27] R.C. Benjamin, D.M. Gill, Poly(ADP-ribose) synthesis in vitro programmed by damaged DNA. A comparison of DNA molecules containing different types of strand breaks, J. Biol. Chem. 255 (1980) 10502–10508.
[28] K. Wielckens, E. George, T. Pless, H. Hilz, Stimulation of poly(ADP-ribosyl)ation during Ehrlich ascites tumor cell "starvation" and suppression of concomitant DNA fragmentation by benzamide, J. Biol. Chem. 258 (1983) 4098–4104.
[29] A. Kreimeyer, K. Wielckens, P. Adamietz, H. Hilz, DNA repair-associated ADP-ribosylation in vivo. Modification of histone H1 differs from that of the principal acceptor proteins, J. Biol. Chem. 259 (1984) 890–896.

[30] R. Alvarez-Gonzalez, F.R. Althaus, Poly(ADP-ribose) catabolism in mammalian cells exposed to DNA-damaging agents, Mutat. Res. 218 (1989) 67–74.
[31] F. Simonin, O. Poch, M. Delarue, G. de Murcia, Identification of potential active-site residues in the human poly(ADP-ribose) polymerase, J. Biol. Chem. 268 (1993) 8529–8535.
[32] L. Tartier, C. Spenlehauer, H.C. Newman, M. Folkard, K.M. Prise, B.D. Michael, J. Menissier-de Murcia, G. de Murcia, Local DNA damage by proton microbeam irradiation induces poly(ADP-ribose) synthesis in mammalian cells, Mutagenesis 18 (2003) 411–416.
[33] F.R. Althaus, C. Richter, ADP-ribosylation of proteins. Enzymology and biological significance, Mol. Biol. Biochem. Biophys. 37 (1987) 1–237.
[34] Y.H. Kang, M.J. Yi, M.J. Kim, M.T. Park, S. Bae, C.M. Kang, C.K. Cho, I.C. Park, M.J. Park, C.H. Rhee, S.I. Hong, H.Y. Chung, Y.S. Lee, S.J. Lee, Caspase-independent cell death by arsenic trioxide in human cervical cancer cells: reactive oxygen species-mediated poly(ADP-ribose) polymerase-1 activation signals apoptosis-inducing factor release from mitochondria, Cancer Res. 64 (2004) 8960–8967.
[35] S. Hanai, M. Kanai, S. Ohashi, K. Okamoto, M. Yamada, H. Takahashi, M. Miwa, Loss of poly(ADP-ribose) glycohydrolase causes progressive neurodegeneration in *Drosophila melanogaster*, Proc. Natl. Acad. Sci. U. S. A. 101 (2004) 82–86.
[36] U. Cortes, W.M. Tong, D.L. Coyle, M.L. Meyer-Ficca, R.G. Meyer, V. Petrilli, Z. Herceg, E.L. Jacobson, M.K. Jacobson, Z.Q. Wang, Depletion of the 110-kilodalton isoform of poly(ADP-ribose) glycohydrolase increases sensitivity to genotoxic and endotoxic stress in mice, Mol. Cell. Biol. 24 (2004) 7163–7178.
[37] N.S. Patel, U. Cortes, R. Di Poala, E. Mazzon, H. Mota-Filipe, S. Cuzzocrea, Z.Q. Wang, C. Thiemermann, Mice lacking the 110-kD isoform of poly(ADP-Ribose) glycohydrolase are protected against renal ischemia/reperfusion injury, J. Am. Soc. Nephrol. 16 (2005) 712–719.
[38] D. Koh, V. Dawson, T. Dawson, The road to survival goes through PARG, Cell Cycle 4 (2005) 397–399.
[39] M. Masutani, H. Nakagama, T. Sugimura, Poly(ADP-ribose) and carcinogenesis, Genes Chromosomes Cancer 38 (2003) 339–348.
[40] W. Ying, M.B. Sevigny, Y. Chen, R.A. Swanson, Poly(ADP-ribose) glycohydrolase mediates oxidative and excitotoxic neuronal death, Proc. Natl. Acad. Sci. U. S. A. 98 (2001) 12227–12232.
[41] H. Chen, D.D. Hughes, T.A. Chan, J.W. Sedat, D.A. Agard, IVE (Image Visualization Environment): a software platform for all three-dimensional microscopy applications, J. Struct. Biol. 116 (1996) 56–60.
[42] G. Carrero, D. McDonald, E. Crawford, G. de Vries, M.J. Hendzel, Using FRAP and mathematical modeling to determine the in vivo kinetics of nuclear proteins, Methods 29 (2003) 14–28.
[43] G. Carrero, E. Crawford, J. Th'ng, G. de Vries, M.J. Hendzel, Quantification of protein–protein and protein–DNA interactions in vivo, using fluorescence recovery after photobleaching, Methods Enzymol. 375 (2004) 415–442.
[44] G. Brochu, G.M. Shah, G.G. Poirier, Purification of poly(ADP-ribose) glycohydrolase and detection of its isoforms by a zymogram following one- or two-dimensional electrophoresis, Anal. Biochem. 218 (1994) 265–272.
[45] N.W. Chi, H.F. Lodish, Tankyrase is a Golgi-associated mitogen-activated protein kinase substrate that interacts with IRAP in GLUT4 vesicles, J. Biol. Chem. 275 (2000) 38437–38444.
[46] J.M. Graham, D. Rickwood, Subcellular Fractionation: A Practical Approach, IRL Press, Oxford, NY, 1997.
[47] G.G. Jonsson, L. Menard, E.L. Jacobson, G.G. Poirier, M.K. Jacobson, Effect of hyperthermia on poly(adenosine diphosphate-ribose) glycohydrolase, Cancer Res. 48 (1988) 4240–4243.
[48] E. Winstall, E.B. Affar, R. Shah, S. Bourassa, I.A. Scovassi, G.G. Poirier, Preferential perinuclear localization of poly(ADP-ribose) glycohydrolase, Exp. Cell Res. 251 (1999) 372–378.
[49] H. Hilz, K. Wielckens, P. Adamietz, R. Bredehorst, A. Kreymeier, Functional aspects of mono- and poly(ADP-ribosyl)ation: subcellular distribution and ADP-ribosyl turnover under conditions of repair and 'starvation', Princess Takamatsu Symp. 13 (1983) 155–163.
[50] H. Maruta, N. Matsumura, S. Tanuma, Role of (ADP-ribose)n catabolism in DNA repair, Biochem. Biophys. Res. Commun. 236 (1997) 265–269.
[51] V.S. Meder, M. Boeglin, G. de Murcia, V. Schreiber, PARP-1 and PARP-2 interact with nucleophosmin/B23 and accumulate in transcriptionally active nucleoli, J. Cell Sci. 118 (2005) 211–222.
[52] J.S. Andersen, C.E. Lyon, A.H. Fox, A.K. Leung, Y.W. Lam, H. Steen, M. Mann, A.I. Lamond, Directed proteomic analysis of the human nucleolus, Curr. Biol. 12 (2002) 1–11.
[53] N. Leitinger, J. Wesierska-Gadek, ADP-ribosylation of nucleolar proteins in HeLa tumor cells, J. Cell. Biochem. 52 (1993) 153–158.
[54] S. Desnoyers, S.H. Kaufmann, G.G. Poirier, Alteration of the nucleolar localization of poly(ADP-ribose) polymerase upon treatment with transcription inhibitors, Exp. Cell Res. 227 (1996) 146–153.
[55] S. Beneke, J. Diefenbach, A. Burkle, Poly(ADP-ribosyl)ation inhibitors: promising drug candidates for a wide variety of pathophysiologic conditions, Int. J. Cancer 111 (2004) 813–818.
[56] S.W. Yu, H. Wang, M.F. Poitras, C. Coombs, W.J. Bowers, H.J. Federoff, G.G. Poirier, T.M. Dawson, V.L. Dawson, Mediation of poly(ADP-ribose) polymerase-1-dependent cell death by apoptosis-inducing factor, Science 297 (2002) 259–263.